

RSC Advances



This is an *Accepted Manuscript*, which has been through the Royal Society of Chemistry peer review process and has been accepted for publication.

Accepted Manuscripts are published online shortly after acceptance, before technical editing, formatting and proof reading. Using this free service, authors can make their results available to the community, in citable form, before we publish the edited article. This *Accepted Manuscript* will be replaced by the edited, formatted and paginated article as soon as this is available.

You can find more information about *Accepted Manuscripts* in the [Information for Authors](#).

Please note that technical editing may introduce minor changes to the text and/or graphics, which may alter content. The journal's standard [Terms & Conditions](#) and the [Ethical guidelines](#) still apply. In no event shall the Royal Society of Chemistry be held responsible for any errors or omissions in this *Accepted Manuscript* or any consequences arising from the use of any information it contains.

1 **One-pot green synthesis of Ag/AgCl nanocubes/reduced graphene oxide and its application**
2 **to the simultaneous determination of hydroquinone and catechol**

3 Ruixue Chen, Qingqing Wang, Yaru Li, Yue Gu, Liu Tang, Cong Li, Zhiquan Zhang*

4 Department of Analytical Chemistry, College of Chemistry, Jilin University, Changchun, 130012,
5 China

6

7

8

9

10

11

12

13

14

15

16

17

18

19

20 *Corresponding author.

21 Tel.: +8618643146598

22 E-mail address: zzq@jlu.edu.cn

1 **Abstract**

2 Uniformly dispersed Ag/AgCl nanocubes (AgNC) were successfully obtained on reduced
3 graphene oxide (rGO) through the simultaneous reduction of Ag⁺ and graphene oxide (GO) by
4 chitosan in the presence of little HCl. The AgCl acted as a seed. The obtained nanocomposite was
5 characterized by X-ray diffraction (XRD), energy dispersive X-ray spectroscopy (EDS) and
6 scanning electron microscopy (SEM). As-synthesized AgNC/rGO was immobilized on the surface
7 of poly (5-amino-1, 3, 4-thiadiazole-2-thiol) (p-ATT) modified carbon fiber disk
8 ultramicroelectrode (CFME) for the simultaneous determination of hydroquinone (HQ) and
9 catechol (CT). This sensor showed a wide linear range of 0.08-1000 $\mu\text{mol L}^{-1}$ for HQ and 1.5-900
10 $\mu\text{mol L}^{-1}$ for CT in the presence of 30 $\mu\text{mol L}^{-1}$ of counterpart.

11

12 Keywords: Ag/AgCl nanocubes/reduced graphene oxide; Carbon fiber disk ultramicroelectrode;
13 Electropolymerization; Hydroquinone; Catechol

14

15

16

17

18

19

20

21

22

1 1. Introduction

2 Silver nanoparticles (AgNP) with unique properties¹ have attracted great attention of chemists in
3 various fields, such as optics,² sensing³ and catalysis.⁴ However, well-dispersed AgNP are difficult to
4 obtain without the use of stabilizers or surfactants because AgNP tend to agglomerate. To resolve the
5 problem, different materials, including silicon nanowires,⁵ multi-walled carbon nanotube,⁶
6 carbonaceous nanospheres⁷ and rGO⁸ have been employed to enhance the stability of AgNP. Among
7 them, rGO has received considerable attention due to its strictly two-dimensional closely packed
8 honeycomb lattice structure, high surface area ($\sim 2600 \text{ m}^2 \text{ g}^{-1}$), high chemical stability and unique
9 electronic, mechanical properties.⁹⁻¹² Many methods have been developed to prepare AgNP/rGO
10 nanocomposite. However, the synthesis of AgNP/rGO nanocomposite is usually based on the
11 reduction of preformed AgNP/GO hybrids or the decoration of rGO sheets with pre-synthesized
12 AgNPs, which involve multiple steps and require complex manipulation.^{13,14} Asiri et al.
13 demonstrated a one-pot hydrothermal reduction method for the preparation of AgNP/rGO hybrids.¹⁵
14 Sun et al. reported a rapid approach to prepare AgNP/rGO sheets using hydrazine hydrate as
15 reducing agent¹⁶. However, these strategies usually require high temperature (more than 100 °C)
16 with high energy-consumption, or suffer from the use of poisonous and hazardous reductant, which
17 may bring about environmental and health risks. Environmentally friendly, cost-effective, and
18 one-step strategy toward rapid preparation of AgNP/rGO nanocomposite attracted attention. The
19 shape-selective catalytic activity could be interpreted in terms of the different reaction performances
20 induced by the specific crystal facets selectively exposed by an anisotropically shaped nanostructure,
21 and also the amount of the catalytically active sites, such as corners, edges, steps, etc. Pan et al.
22 anchored hexagonal Ag nanoplates to rGO to form novel Ag nanoplates/rGO nanocomposite.¹⁷ Jiang
23 et al. prepared silver nanorod/reduced graphene oxide by the chemical-microwave reduced

1 procedure.¹⁸ Chen et al. synthesized silver nanowire-decorated reduced graphene oxide nanosheets
2 with the aid of trisodium citrate.¹⁹ Among various shapes, nanocubes have exhibited extremely high
3 electrocatalytic activity due to its rich (1 0 0) facets.²⁰ For example, Yang et al. reported an
4 amperometric bienzyme glucose biosensor by co-immobilization HRP and GOx on the Ag
5 nanocubes.²¹ Yang et al. developed an amperometric non-enzymatic glucose sensor by
6 electrodepositing copper nanocubes onto vertically well-aligned multi-walled carbon nanotube
7 arrays.²² To the best of our knowledge, no literatures are reported for the preparation of AgNC/rGO.
8 Lu et al. synthesized four different morphologies of silver nanoproducts by altering the
9 concentration of Na₂S.²³ Liu et al. facilely formulated AgCl nanocubes in terms of hybridizing GO.²⁴
10 Based on these, we want to synthesize AgNC/rGO. GO works as a capping agent during the
11 nanofabrication step. Chitosan is derivative of the polysaccharide chitin widely distributed in nature
12 and a large number of free amino and hydroxyl groups in chitosan chains offering unique
13 physicochemical properties. In this paper, taking advantage of the reducing ability of chitosan
14 towards AgNO₃²⁵ and GO,²⁶ a green one-pot method for growing Ag/AgCl nanocubes on rGO is
15 developed by simultaneous reduction of AgNO₃ and GO with chitosan in the presence of little HCl.
16 Hydroquinone (HQ) and catechol (CT) are two important isomers of dihydroxybenzene, which
17 are frequently used as industrial reagents in the production of rubber, dyes, plastics, pharmaceuticals
18 and cosmetics. They widely exist in environment as a kind of important pollutant because they are
19 toxic to humans and difficult to be degraded. What is more, due to their similar structures and
20 properties, HQ and CT usually coexist in products and interfere with each other during their
21 identification.²⁷ Several methods have been exploited for the determination of HQ and CT, such as
22 chemiluminescence,²⁸ liquid chromatography,²⁹ spectrophotometry,³⁰ synchronous fluorescence

1 technique³¹ and electrochemical methods.³² Among them, electrochemical methods have attracted
2 more and more attentions due to the advantages of fast response, cheap instrument, low cost, simple
3 operation, time-saving, high sensitivity and excellent selectivity. Various electrodes were used for
4 the determination of HQ and CT such as glassy carbon electrode,³³ platinum electrode³⁴ and carbon
5 electrode.³⁵ However, they couldn't distinguish HQ and CT directly because HQ and CT have similar
6 structures and properties. Zhang et al. developed boron-doped rGO modified glassy carbon electrode
7 for the determination of HQ and CT.³⁶ Wang et al. presented multiwall carbon
8 nanotubes-poly(diallyldimethylammonium chloride)-rGO modified glassy carbon electrode for the
9 simultaneous detection of HQ and CT.³⁷ Kashanian described a method for construction of an
10 electrochemical biosensor to detect CT based on covalent immobilization of laccase onto polyaniline
11 electrodeposited onto a glassy carbon electrode.³⁸ Li et al. fabricated an electrochemical sensor
12 based on disulfides bridged β -cyclodextrin dimer-functionalized multi-walled carbon nanotube for
13 simultaneous determination of 4-Aminophenol, 4-Chlorophenol and 4-Nitrophenol.³⁹ Srivastava et
14 al. reported the synthesis of AgNP/rGO in the presence of sodium hydroxide, and AgNP/rGO based
15 electrochemical sensor was fabricated for the simultaneous determination of ascorbic acid, dopamine,
16 uric acid, and tryptophan.⁴⁰ The application of AgNC/rGO and CFME for electrochemical sensors of
17 HQ and CT has rarely been explored. In the present study, we find that CFME, which has excellent
18 intrinsic characteristics such as temporal resolution, high current densities and reduced ohmic drop,
19 can achieve their simultaneous determination on bare electrode. Conjugated polymers derive from
20 heterocyclic compounds have emerged as promising materials for immobilizing nanomaterial due to
21 their conducting nature and high stability. In this work, we electrodeposited ATT onto CFME for the
22 first time. The $-NH_2$ and $-SH$ groups exposed to the p-ATT can facilitate the immobilizing of

1 AgNC/rGO. Considering above, AgNC/rGO/p-ATT modified CFME was developed for the
2 simultaneous and sensitive determination of HQ and CT, where the high electron transfer ability of
3 p-ATT was combined with the unique electronic structure of AgNC/rGO. This sensor showed a good
4 electrocatalytic performance to HQ and CT with wide linear range, low detection limit, good
5 stability and reproducibility.

6 **2. Experimental**

7 **2.1. Reagents and apparatus**

8 Chitosan with a deacetylation degree of 90% was purchased from Sinopharm Chemical Regent
9 Co. Ltd, used as received. AgNO₃ was purchased from Tianjin Damao Chemical Factory. All other
10 chemicals were of analytical grade from Shanghai Chemical Factory (Shanghai, China), and all
11 solutions were prepared with distilled water.

12 The morphologies of the samples were observed using a scanning electron microscope (SEM,
13 Hitachi S-4800) with energy dispersive X-ray spectrometry (EDS) mode. The crystal structures of
14 the samples were examined by X-ray diffraction (XRD; D/max2550VB X-ray diffractometer,
15 Rigaku).

16 Electrochemical measurements were performed on a CHI-920c workstation (CH Instruments).
17 A Faraday cage was used to reduce electrical noise. A three-electrode configuration consisted of a
18 carbon fiber disk ultramicroelectrode, a platinum wire, and saturated calomel electrode (SCE) as
19 the working, the counter and the reference electrodes, respectively. All potentials in this work are
20 referred to SCE as the reference.

21 **2.2. Preparation of AgNC/rGO nanocomposite**

22 GO was obtained by oxidizing graphite using an improved method published by Marcano et

1 al.⁴¹ A stock solution of 1% chitosan was prepared by dissolving chitosan in 0.5 mol L⁻¹ acetic
2 acid solution. 4 mL AgNO₃ solution (26 mmol L⁻¹) was added to the stirring GO suspension (10
3 mL, 0.5 mg mL⁻¹, pH = 6 adjust with HCl). Then, they were added to the chitosan solution (20
4 mL). Subsequently, the mixture was kept at 95°C for 3 days. Upon the reaction, the suspension
5 changed its color from light brown to dark, suggesting the formation of AgNC/rGO
6 nanocomposite. The solid product was isolated by centrifugation.

7 **2.3. Preparation of AgNC/rGO/p-ATT/CFME**

8 CFME was fabricated according to the reported method with some modifications.⁴² A single
9 carbon fiber (5 μm diameter) was inserted into the tip of the glass tube (1~2 mm diameter) and
10 filled with epoxy resin. After drying, graphite and copper wire were inserted for electrical contact.
11 The microelectrode surface was polished mechanically with graded alumina powder of different
12 sizes (1, 0.3, 0.05 μm) on a polishing cloth. The response of polished electrodes was tested by
13 voltammetry in 0.1 mol L⁻¹ KCl containing 10 mmol L⁻¹ K₃[Fe(CN)₆] at a scan rate of 10 mV s⁻¹.
14 Due to its well-established behavior, the voltammograms exhibited sigmoid profiles characteristic
15 of the utilization of microelectrodes.⁴³

16 Electropolymerization of ATT onto the CFME was carried out by using cyclic voltammetry. 15
17 successive potential sweeps were applied between -0.40 and +1.70 V at a scan rate of 50 mV s⁻¹ in
18 0.10 mol L⁻¹ H₂SO₄ containing 1.0 mmol L⁻¹ ATT. The CV of electrochemical polymerized ATT
19 was similar but lower ATT oxidation and reduction signal comparing with the earlier report.⁴⁴
20 Then, the CFME was dipped for 30 min in 0.5 mg mL⁻¹ AgNC/rGO solution and dried in air
21 before use.

22 **3. Results and discussion**

3.1. Characterization of AgNC/rGO

Using chitosan as a reducing reagent to prepare AgNC/rGO is simple and can't introduce any environmental toxicity. The XRD pattern was used to identify the formation of AgNC/rGO (Fig. 1). Graphite powder shows a sharp peak at 26.4° with a typical interlayer spacing of 0.34 nm (curve a). The XRD pattern shows a sharp peak at 2θ of 9.6° (curve b), which can be ascribed to the characteristic diffraction peak of GO. It is corresponding to a layer-to-layer distance (d-spacing) of about 0.86 nm. This is larger than that of pristine graphite (0.34 nm), as a result of the introduction of oxygenated functional groups on carbon sheets. After being reduced by chitosan, the diffraction peaks at 2θ of 37.7 (1 1 1), 44.3 (2 0 0), 64.4 (2 2 0) and 77.3 (3 1 1) correspond to the cubic phase of Ag (JCPDS No. 65-2871). The intensity ratio of the (2 0 0) to (1 1 1) peak is 0.644, which is higher than the value (i.e., 0.4) detected in conventional powder samples (JCPDS card file No. 04-0783), indicating that the silver nanostructures are growing preferentially along the (1 0 0) direction and the sides of the silver cubes are bound by the enlarged (1 0 0) facets. The XRD result manifests the fcc silver crystal feature of the synthesized nanocubes²⁰. The peaks at 2θ of 27.6 (1 1 1), 32.4 (2 0 0), 46.1 (2 2 0), 54.8 (3 1 1) and 57.4 (2 2 2) can be assigned to the cubic phase of AgCl (JCPDS No. 31-1238) (curve c). The XRD result indicates the coexistence of Ag and AgCl in our nanocomposite. The low intensity for the diffraction peaks of AgCl may be due to the low content. No diffraction peak attributed to rGO is found. This is because the anchored AgNC disrupt the layered and ordered structure of rGO, and consequently lead to the disappearance of the reflection peak.

In addition, the existence of both rGO and AgNC can be indicated from peaks of energy dispersive X-ray spectroscopy (EDS). The EDS spectrum suggests that nanocomposite consists of

1 Ag, Cl, C, O and Si elements. The result shows that the nanocomposite is composed of Ag and
2 AgCl with a molar ratio of 4.65:1 (Fig. 2), which is consistent with the result of XRD. The Si
3 signal derives from the silicon chip. Reduction of GO with chitosan does not generate perfect
4 graphene, and few oxygen-containing groups (OCGs) still remain in the rGO owing to the limited
5 restoring ability of reductions.⁴⁵ The residual OCGs have the opportunity to capture the amino and
6 hydroxyl groups of chitosan via zwitterionic interaction and hydrogen bonding, by which chitosan
7 noncovalently bond to the rGO and endows with dispersibility in water.⁴⁶ Therefore, we had
8 successfully synthesized AgNC/rGO.

9 The morphologies of GO and AgNC/rGO are characterized by SEM. The SEM image of GO
10 (Fig. 3A) depicts wrinkled structures, explicating the intrinsic GO morphology. The SEM image of
11 the AgNC/rGO (Fig. 3B) reveals that large quantities of AgNC with the size of about 100 nm are
12 attached on the silk-like surface of the rGO. The wrinkles appearing on the surface of the particles
13 could illustrate the existence of rGO.

14 Fig. 4 shows the cyclic voltammograms of different electrodes in the 10.0 mmol L⁻¹
15 K₃[Fe(CN)₆] containing 0.1 mol L⁻¹ KCl. According to Tomes criterion for a reversible system,
16 this potential difference ($E_{3/4} - E_{1/4}$) should be 54.4/n mV at 298 K where n is the number of
17 electrons transferred during the electrochemical process. Bare CFME showed that this potential
18 difference is 46 mV. The value is close to the expected value, which indicated that reversible
19 system was obtained on the bare CFME. Compared to the bare CFME, the peak current of
20 p-ATT/CFME increased, which could be attributed to the excellent electrical conductivity and fast
21 electron transfer rate of p-ATT. The peak current of K₃[Fe(CN)₆] at AgNC/rGO/CFME was higher
22 than the peak current at the bare CFME, which was due to the good electrical conductivity and

1 catalyst effect of AgNC/rGO. The AgNC/rGO/p-ATT/CFME showed the biggest peak current
2 compared to bare CFME and p-ATT/CFME. The result could be attributed to the synergistic
3 effects of p-ATT and AgNC/rGO, which improved the whole interfacial conductivity.

4 **3.2. Electrochemical behaviors of HQ and CT at AgNC/rGO/p-ATT/CFME**

5 Among the electroanalytical techniques for use with microelectrodes, square-wave voltammetry
6 (SWV) has proved to be extremely sensitive for the detection of organic molecules.⁴⁷ The
7 electrocatalytic activity of the AgNC/rGO/p-ATT film was evaluated by the comparison of SWVs
8 of 300 $\mu\text{mol L}^{-1}$ HQ and CT in pH 5.0 acetate buffer recorded at four different working electrodes
9 (Fig. 5). Two peaks are presented at potentials of 0.154 and 0.284 V, which correspond to the
10 oxidation peaks of HQ and CT on bare CFME (curve a). The electron cloud density of HQ is
11 lower than that of CT, so CT is harder to be oxidized than HQ. The resultant separation in two
12 peak potentials (about 130 mV) is sufficient enough to achieve the simultaneous determination of
13 HQ and CT in their mixtures. At the AgNC/rGO/CFME (curve b), the peaks current of HQ and CT
14 are higher than that of the bare CFME, which should be due to the high surface area and excellent
15 electrical conductivity of AgNC/rGO. At the p-ATT/CFME (curve c), intensive increases in peak
16 currents of both HQ and CT are obtained. The catalytic effect is attributed to the following reasons:
17 on the one hand, polymer film has the hydrophobic interaction with the aromatic part of analysts;
18 on the other hand, the pKa values of HQ and CT are 9.85 and 9.4, respectively. At pH 5.0, -NH₂
19 and -SH groups exposed to the p-ATT layer and the ionized hydroxyl in dihydroxybenzenes
20 increase the adsorption capacity of the three dihydroxybenzene isomers.⁴⁸ As for
21 AgNC/rGO/p-ATT/CFME, the peak currents of HQ and CT are 5.6 and 3.7 times of the bare
22 CFME (curve d). The excellent performance may attribute to the following reasons:

- 1 (1) p-ATT film is highly conducting and its redox kinetics are fast.⁴⁴
- 2 (2) The high density of localize π electrons in rGO surface would be beneficial for the
- 3 accumulation of HQ and CT through the strong π - π interactions.
- 4 (3) AgNC/rGO can provide larger electrochemical active surface areas and effectively accelerate
- 5 the electron transfer between electrode and analytes.
- 6 In summary, synergistic effect of above reasons makes AgNC/rGO/p-ATT/CFME possible as an
- 7 electrochemical sensor for simultaneous and sensitive determination of HQ and CT.

8 **3.3. Influence of solution pH and scan rate**

9 The effect of pH on the peak potential and current of HQ and CT at AgNC/rGO/p-ATT/CFME

10 was also investigated in 0.2 mol L⁻¹ acetate buffer solutions by SWV in the pH range of 3.0-7.0.

11 As seen from Fig. 6A, the peak potentials for HQ and CT display a same trend and shift almost

12 linearly toward negative potential when pH increased from 3.0 to 7.0, suggesting that protons have

13 directly taken part in the electrode reaction process of both HQ and CT. Accordingly, HQ is more

14 sensitive to respond oxidation even at low concentration as compared to CT. The maximal peak

15 current for HQ is obtained at pH 6.0, and the maximal peak current for CT is obtained at pH 5.0.

16 In order to determine HQ and CT sensitively, all experiments were carried out at pH 5.0. The

17 dependence of E_p on pH can be represented by the equations (Fig. 6B):

18 HQ: $E_p = 0.48 - 0.06\text{pH}$ (1)

19 CT: $E_p = 0.549 - 0.055\text{pH}$ (2)

20 The two almost parallel lines indicate that the peak potential difference between HQ and CT is

21 constant. According to the following formula:

22 $dE_p/d\text{pH} = -2.303mRT/nF$ ⁴⁹ (3)

1 'm' and 'n' are the number of proton and electron, respectively; 'm/n' is calculated to be 1.01 and
2 0.93 for the HQ and CT oxidation process, respectively. It means the number of proton and
3 electron involved in the oxidative process of HQ and CT is equal. In addition, the slopes of the
4 regression equations are close to the theory value of 58.5 mV pH⁻¹ for two electrons and two
5 protons process.⁵⁰ The probable electrode reaction is shown in Scheme 1.

6 The reaction kinetic was investigated by studying the effects of scan rate dependence toward the
7 oxidation peak current of 300 μmol L⁻¹ HQ and CT in acetate buffer (pH 5.0) (Fig. 7). With the
8 increase of scan rate from 30 to 380 mV s⁻¹, the anodic peak currents increased linearly with the
9 square root of scan rates, following the regression equation:

10 HQ: $I_p = 0.10366v^{1/2} - 0.5296$ (R=0.993) (4)

11 CT: $I_p = 0.05863v^{1/2} - 0.1293$ (R=0.990) (5)

12 This indicated that the electrode reaction of HQ and CT on AgNC/rGO/p-ATT/CFME was a
13 typical diffusion-controlled process. The E_p shifted positively along with the increase of scan rate,
14 showing a linear relationship with log v (Fig. 7D), which was further constructed with the
15 equation:

16 HQ: $E_p = 0.130\log v + 0.412$ (R=0.993) (6)

17 CT: $E_p = 0.112\log v + 0.45$ (R=0.990) (7)

18 According to the following formula:

19 $E_p = A + 2.303RT \log v / (1 - \alpha)nF$ (8)

20 'A' is a constant; 'α' is the transfer coefficient characterizes; 'n' is the number of electrons
21 involved in the rate-controlling step; 'R', 'T' and 'F' are the gas constant, temperature and Faraday
22 constant, respectively. On the basis of the slope being equal to 2.303RT/(1 - α)nF, the

1 transferred electron was calculated to be 1.58 for HQ and 1.76 for CT ($\alpha = 0.7$), suggesting that
2 two electrons were involved in the oxidation reaction. The result was consistent with Scheme 1.

3 **3.4. Determination of HQ and CT by square-wave voltammetry**

4 Under the optimal conditions, the determination of HQ and CT at AgNC/rGO/p-ATT/CFME
5 was carried out by SWV, where the concentration of one species changed while the other one
6 remained constant. As shown in Fig. 8A, keeping the concentration of CT constant ($30 \mu\text{mol L}^{-1}$),
7 the oxidation peak current increases linearly with increasing the concentration of HQ in the range
8 of $0.08\text{-}1000 \mu\text{mol L}^{-1}$. The regression equation is described as:

$$9 \log I_p = 0.725 \log C - 0.88752 \quad (R = 0.997) \quad (9)$$

10 Similarly, as shown in Fig. 8B, the peak current linearly increases with increasing concentration of
11 CT from 1.5 to $900 \mu\text{mol L}^{-1}$, while keeping the concentration of HQ constant at $30 \mu\text{mol L}^{-1}$. The
12 regression equation is described as:

$$13 \log I_p = 0.731 \log C - 3.7683 \quad (10)$$

14 The determination limits were calculated from the calibration curve using the $3s_b/m$, where s_b is
15 the standard deviation of the intercept and m is the slope of the calibration graph.⁵¹ The detection
16 limits of HQ and CT are shown in Table 1. The peak current of CT kept almost constant as HQ
17 concentration was increased, further confirming that this modified electrode can be employed for
18 the simultaneous determination of HQ and CT without interference with each other. The present
19 results are compared to those in literatures (Table 2). It shows that the linear range of HQ and CT
20 at the present work are much wider, and the detection limit is lower than that in previously
21 published works. We used CFME to determine HQ and CT, which can be used in vivo. The RSD
22 of regression equation is similar with other sensors, which demonstrates the good linear

1 relationship between logarithm of concentrations and logarithm of the current.

2 **3.5. Reproducibility, stability of AgNC/rGO/p-ATT/CFME and interference studies**

3 Besides the sensitivity and selectivity, reproducibility and stability are important parameters to
4 evaluate the applicability of electrochemical sensor. To characterize the reproducibility of the
5 AgNC/rGO/p-ATT/CFME, 6 consecutive measurements were done for 300 $\mu\text{mol L}^{-1}$ HQ and CT
6 at the same electrode. The relative standard deviation (RSD) was 0.9% and 2.1% for HQ and CT,
7 revealing that the AgNC/rGO/p-ATT/CFME sensing device had good reproducibility. The long
8 term stability of the AgNC/rGO/p-ATT/CFME sensing device was also examined by measuring
9 SWV peak currents of 300 $\mu\text{mol L}^{-1}$ HQ and CT after storing the electrode for 10 days. After 10
10 days, the AgNC/rGO/p-ATT/CFME sensing device retained 91% of the original values,
11 demonstrating that the sensing device had better long term stability. These results revealed the
12 appreciable reproducibility and good stability of the proposed sensor. The possible interferences of
13 some inorganic ions and organic compounds were investigated with a mixed dihydroxybenzenes
14 solution (HQ and CT, each 300 $\mu\text{mol L}^{-1}$) by SWV. It was found that 100-fold Na^+ , K^+ , NH_4^+ ,
15 Mg^{2+} , Cl^- , SO_4^{2-} , glycine, ethanol, glucose and ascorbic acid, 10-fold Ca^{2+} , Fe^{2+} , Cu^{2+} , H_2PO_4^- and
16 2-fold nitrophenol, resorcinol and phenol did not interfere with the determination (signals change
17 below 5.0%), indicating good antiinterference ability of AgNC/rGO/p-ATT modified CFME.

18 **3.6. Water samples analysis**

19 To demonstrate the practical application of AgNC/rGO/p-ATT/CFME for the simultaneous
20 determination of HQ and CT, local lake water and tap water samples were tested. The
21 determination of the HQ and CT concentration was performed by the standard addition method.
22 The lake water samples were obtained from South Lake (Changchun, China), and they were

1 determined after certain volume of pH 5.0 acetate buffer was introduced. The obtained results are
2 listed in Table 3, which indicate the direct determination of HQ and CT in water is possible after
3 dilution of the sample with the supporting electrolyte.

4 **4. Conclusions**

5 In order to prepare Ag/AgCl nanocubes/reduced graphene oxide, we used AgCl as crystal seed.
6 Uniformly dispersed Ag/AgCl nanocubes were successfully obtained on rGO using chitosan as
7 reductant, employing AgNO₃ and GO as starting materials in the presence of HCl. The reduction
8 of GO and the generation of the Ag/AgCl nanocubes occurred simultaneously. The merit of this
9 method lies in its low-cost, non use of toxic agent and easily scalable. Ag/AgCl
10 nanocubes/reduced graphene oxide showed high stability and dispersity in water and large surface
11 area, and had been successfully applied in catalytic performance toward the oxidation of HQ and
12 CT. AgNCs/rGO/p-ATT/CFME showed a wide linear concentration range (0.08-1000 μmol L⁻¹ for
13 HQ and 1.5-900 μmol L⁻¹ for CT) and a low detection limit (0.0094 μmol L⁻¹ for HQ and 0.13
14 μmol L⁻¹ for CT), indicating that AgNC/rGO/p-ATT/CFME could be utilized as a promising
15 sensing platform for the determination of HQ and CT.

16 **Acknowledgements**

17 This work was supported by the NNSFC (No. 21375045) and NSF of Jilin Province (No.
18 20130101118JC).

19

20

21

22

1 **References**

- 2 1 B. Wiley, Y. Sun and Y. Xia, *Accounts of Chemical Research*, 2007, **40**, 1067-1076.
- 3 2 Z. Xu, Y. Hou and S. Sun, *Journal of the American Chemical Society*, 2007, **129**, 8698-8699.
- 4 3 H. Wang, X. Zheng, J. Chen, D. Wang, Q. Wang, T. Xue, C. Liu, Z. Jin, X. Cui and W. Zheng,
5 *Journal of Physical Chemistry C*, 2012, **116**, 24268-24273.
- 6 4 P. Christopher, H. Xin and S. Linic, *Nature Chemistry*, 2011, **3**, 467-472.
- 7 5 M. Lv, S. Su, Y. He, Q. Huang, W. Hu, D. Li, C. Fan and S. T. Lee, *Advanced Materials*, 2010,
8 **22**, 5463-5467.
- 9 6 P. Gunawan, C. Guan, X. Song, Q. Zhang, S. S. J. Leong, C. Tang, Y. Chen, M. B. Chan-Park, M.
10 W. Chang, K. Wang and R. Xu, *Acs Nano*, 2011, **5**, 10033-10040.
- 11 7 J. Cui, C. Hu, Y. Yang, Y. Wu, L. Yang, Y. Wang, Y. Liu and Z. Jiang, *Journal of Materials*
12 *Chemistry*, 2012, **22**, 8121-8126.
- 13 8 J. D. Kim, T. Palani, M. R. Kumar, S. Lee and H. C. Choi, *Journal of Materials Chemistry*, 2012,
14 **22**, 20665-20670.
- 15 9 A. K. Geim, *science*, 2009, **324**, 1530-1534.
- 16 10 F. Schedin, A. Geim, S. Morozov, E. Hill, P. Blake, M. Katsnelson and K. Novoselov, *Nature*
17 *Materials*, 2007, **6**, 652-655.
- 18 11 M. I. Katsnelson, *Materials Today*, 2007, **10**, 20-27.
- 19 12 K. S. Kim, Y. Zhao, H. Jang, S. Y. Lee, J. M. Kim, K. S. Kim, J. H. Ahn, P. Kim, J. Y. Choi and
20 B. H. Hong, *Nature*, 2009, **457**, 706-710.
- 21 13 R. Pasricha, S. Gupta and A. K. Srivastava, *Small*, 2009, **5**, 2253-2259.
- 22 14 J. Liu, S. Fu, B. Yuan, Y. Li and Z. Deng, *Journal of the American Chemical Society*, 2010, **132**,

- 1 7279-7281.
- 2 15 X. Qin, Y. Luo, W. Lu, G. Chang, A. M. Asiri, A. O. Al-Youbi and X. Sun, *Electrochimica Acta*,
- 3 2012, **79**, 46-51.
- 4 16 S. Liu, L. Wang, J. Tian, Y. Luo, X. Zhang and X. Sun, *Journal of colloid and interface science*,
- 5 2011, **363**, 615-619.
- 6 17 L. Huang, K. Hou, X. Jia, H. Pan and M. Du, *Materials Science and Engineering: C*, 2014, **38**,
- 7 39-45.
- 8 18 Q. Liu, X. Zhang, G. Wen, Y. Luo, A. Liang and Z. Jiang, *Plasmonics*, 2015, **10**, 285-295.
- 9 19 J. Tang, D. Tang, B. Su, Q. Li, B. Qiu and G. Chen, *Electrochimica Acta*, 2011, **56**, 8168-8175.
- 10 20 S. Qi, X. Shen, Z. Lin, G. Tian, D. Wu and R. Jin, *Nanoscale*, 2013, **5**, 12132-12135.
- 11 21 P. Yang, L. Wang, Q. Wu, Z. Chen and X. Lin, *Sensors and Actuators B: Chemical*, 2014, **194**,
- 12 71-78.
- 13 22 J. Yang, W. D. Zhang and S. Gunasekaran, *Biosensors & Bioelectronics*, 2010, **26**, 279-284.
- 14 23 J. Geng, Y. Bi and G. Lu, *Electrochemistry Communications*, 2009, **11**, 1255-1258.
- 15 24 M. Zhu, P. Chen and M. Liu, *Langmuir*, 2013, **29**, 9259-9268.
- 16 25 H. V. Tran, L. D. Tran, C. T. Ba, H. D. Vu, T. N. Nguyen, D. G. Pham and P. X. Nguyen,
- 17 *Colloids and Surfaces A: Physicochemical and Engineering Aspects*, 2010, **360**, 32-40.
- 18 26 Y. Guo, X. Sun, Y. Liu, W. Wang, H. Qiu and J. Gao, *Carbon*, 2012, **50**, 2513-2523.
- 19 27 X. Zhang, S. Duan, X. Xu, S. Xu and C. Zhou, *Electrochimica Acta*, 2011, **56**, 1981-1987.
- 20 28 Y. G. Sun, H. Cui, Y. H. Li and X. Q. Lin, *Talanta*, 2000, **53**, 661-666.
- 21 29 H. Cui, C. X. He and G. W. Zhao, *Journal of Chromatography A*, 1999, **855**, 171-179.
- 22 30 P. Nagaraja, R. A. Vasantha and K. R. Sunitha, *Journal of Pharmaceutical and Biomedical*

- 1 *Analysis*, 2001, **25**, 417-424.
- 2 31 M. F. Pistonesi, M. S. Di Nezio, M. Centurion, M. E. Palomeque, A. G. Lista and B. S. F. Band,
- 3 *Talanta*, 2006, **69**, 1265-1268.
- 4 32 C. Wang, Y. Chen, K. Zhuo and J. Wang, *Chemical Communications*, 2013, **49**, 3336-3338.
- 5 33 F. Hu, S. Chen, C. Wang, R. Yuan, D. Yuan and C. Wang, *Analytica Chimica Acta*, 2012, **724**,
- 6 40-46.
- 7 34 X. Feng, Y. Shi and Z. Hu, *Materials Chemistry and Physics*, 2011, **131**, 72-76.
- 8 35 X. Hu, J. Li and J. Wang, *Electrochemistry Communications*, 2012, **21**, 73-76.
- 9 36 Y. Zhang, R. Sun, B. Luo and L. Wang, *Electrochimica Acta*, 2015, **156**, 228-234.
- 10 37 D. Song, J. Xia, F. Zhang, S. Bi, W. Xiang, Z. Wang, L. Xia, Y. Xia, Y. Li and L. Xia, *Sensors*
- 11 *and Actuators B: Chemical*, 2015, **206**, 111-118.
- 12 38 M. Nazari, S. Kashanian and R. Rafipour, *Spectrochimica Acta Part A: Molecular and*
- 13 *Biomolecular Spectroscopy*, 2015, **145**, 130-138.
- 14 39 L. Yang, S. Fan, G. Deng, Y. Li, X. Ran, H. Zhao and C. P. Li, *Biosensors and Bioelectronics*,
- 15 2015, **68**, 617-625.
- 16 40 B. Kaur, T. Pandiyan, B. Satpati and R. Srivastava, *Colloids and Surfaces B: Biointerfaces*,
- 17 2013, **111**, 97-106.
- 18 41 D. C. Marcano, D. V. Kosynkin, J. M. Berlin, A. Sinitskii, Z. Sun, A. Slesarev, L. B. Alemany,
- 19 W. Lu and J. M. Tour, *Acs Nano*, 2010, **4**, 4806-4814.
- 20 42 M. Kathiwala, A. O. Affum, J. Perry and A. Brajter-Toth, *Analyst*, 2008, **133**, 810-816.
- 21 43 T. M. Oliveira, H. Becker, E. Longhinotti, D. De Souza, P. de Lima-Neto and A. N. Correia,
- 22 *Microchemical journal*, 2012, **109**, 84-92.

- 1 44 P. Kalimuthu and S. A. John, *Electrochemistry Communications*, 2009, **11**, 367-370.
- 2 45 D. Li, M. B. Muller, S. Gilje, R. B. Kaner and G. G. Wallace, *Nature Nanotechnology*, 2008, **3**,
- 3 101-105.
- 4 46 M. Fang, L. A. Long, W. F. Zhao, L. W. Wang and G. H. Chen, *Langmuir*, 2010, **26**,
- 5 16771-16774.
- 6 47 M. R. C. Massaroppi, S. A. S. Machado and L. A. Avaca, *Journal of the Brazilian Chemical*
- 7 *Society*, 2003, **14**, 113-119.
- 8 48 P. Kalimuthu and S. A. John, *Bioelectrochemistry*, 2009, **77**, 13-18.
- 9 49 E. Laviron, *Journal of Electroanalytical Chemistry and Interfacial Electrochemistry*, 1974, **52**,
- 10 355-393.
- 11 50 B. J. Sanghavi and A. K. Srivastava, *Electrochimica Acta*, 2010, **55**, 8638-8648.
- 12 51 P. N. Bartlett, E. Ghoneim, G. El-Hefnawy and I. El-Hallag, *Talanta*, 2005, **66**, 869-874.
- 13 52 M. U. Anu Prathap, B. Satpati and R. Srivastava, *Sensors and Actuators B: Chemical*, 2013,
- 14 **186**, 67-77.
- 15 53 W. Si, W. Lei, Y. Zhang, M. Xia, F. Wang and Q. Hao, *Electrochimica Acta*, 2012, **85**, 295-301.
- 16 54 J. Qu, Y. Wang, J. Guo, Y. Dong and T. Lou, *Journal of The Electrochemical Society*, 2014, **161**,
- 17 B220-B224.
- 18 55 L. Zheng, L. Xiong, Y. Li, J. Xu, X. Kang, Z. Zou, S. Yang and J. Xia, *Sensors and Actuators B:*
- 19 *Chemical*, 2012, **177**, 344-349.
- 20 56 H. L. Guo, S. Peng, J. H. Xu, Y. Q. Zhao and X. Kang, *Sensors and Actuators B: Chemical*,
- 21 2014, **193**, 623-629.
- 22 57 S. Hu, W. Zhang, J. Zheng, J. Shi, Z. Lin, L. Zhong, G. Cai, C. Wei, H. Zhang and A. Hao, *RSC*

1 *Advances*, 2015, **5**, 18615-18621.

2

3

4

5

6

7

8

9

10

11

12

13

14

15

16

17

18

19

20

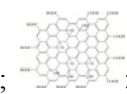
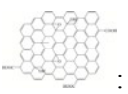
21

22

RSC Advances Accepted Manuscript

1 **Captions**

2 **Scheme 1.** Mechanism of oxidative reactions of HQ and CT at AgNC/rGO/p-ATT modified

3  CFME;  :GO,  : rGO,  : Ag⁺,  : chitosan,  : AgNC.

4 **Fig. 1.** XRD patterns of the (a) graphite, (b) GO, and (c) AgNC/rGO composite.

5 **Fig. 2.** EDS spectrum of AgNC/rGO.

6 **Fig. 3.** SEM images of the (A) GO, and (B) AgNC/rGO composite.

7 **Fig. 4.** Cyclic voltammograms of 10.0 mmol L⁻¹ K₃[Fe(CN)₆] containing 0.1 mol L⁻¹ KCl at bare
8 CFME, p-ATT/CFME, AgNC/rGO/CFME, and AgNC/rGO/p-ATT/CFME.

9 **Fig. 5.** Square-wave voltammetry for 300 μmol L⁻¹ HQ and CT in acetate buffer (pH 5.0) on the
10 surface of various electrodes: curve (a) CFME, (b) AgNC/rGO/CFME, (c) p-ATT/CFME, and (d)
11 AgNC/rGO/p-ATT/CFME.

12 **Fig. 6.** (A) Square-wave voltammetry of AgNC/rGO/p-ATT/CFME for 300 μmol L⁻¹ HQ and CT
13 in 0.2 mol L⁻¹ acetate buffer with different pH values; (B) the dependence of peak potentials of
14 HQ and CT on the pH of the buffer at AgNC/rGO/p-ATT/CFME.

15 **Fig. 7.** Influence of scan rate on the peak currents of 300 μmol L⁻¹ HQ (A) and CT (B) at
16 AgNC/rGO/p-ATT/CFME in 0.2 mol L⁻¹ acetate buffer solution (pH 5.0): 30, 50, 80, 100, 130,
17 150, 180, 200, 230, 250, 280, 300, 330, 350, and 380 mV s⁻¹; (C) Plot of peak currents of HQ and
18 CT versus square roots of scan rate; (D) plot of peak potentials of HQ and CT versus logarithm of
19 scan rate.

20 **Fig. 8.** Square-wave voltammetry at AgNC/rGO/p-ATT/CFME in 30 μmol L⁻¹ CT and different
21 concentrations of HQ: 0.08, 0.3, 0.7, 5, 10, 20, 50, 100, 200, 300, 400, 500, 600, 700, 800, 900,
22 and 1000 μmol L⁻¹ (A); (B) 30 μmol L⁻¹ HQ and different concentrations of CT: 1.5, 5, 20, 50, 100,

1 200, 300, 400, 500, 600, 700, 800, and 900 $\mu\text{mol L}^{-1}$; Calibration curves from logarithm of the
2 current response at AgNC/rGO/p-ATT/CFME vs. logarithm of concentrations of HQ (C) and CT
3 (D) in acetate buffer solutions (pH 5.0).

4 **Table 1**

5 Results obtained from the linear regression.

6 **Table 2**

7 Performance comparison of the fabricated electrode for HQ and CT detection with other
8 electrodes.

9 **Table 3**

10 Recovery of HQ and CT in different water samples at AgNC/rGO/p-ATT/CFME.

11

12

13

14

15

16

17

18

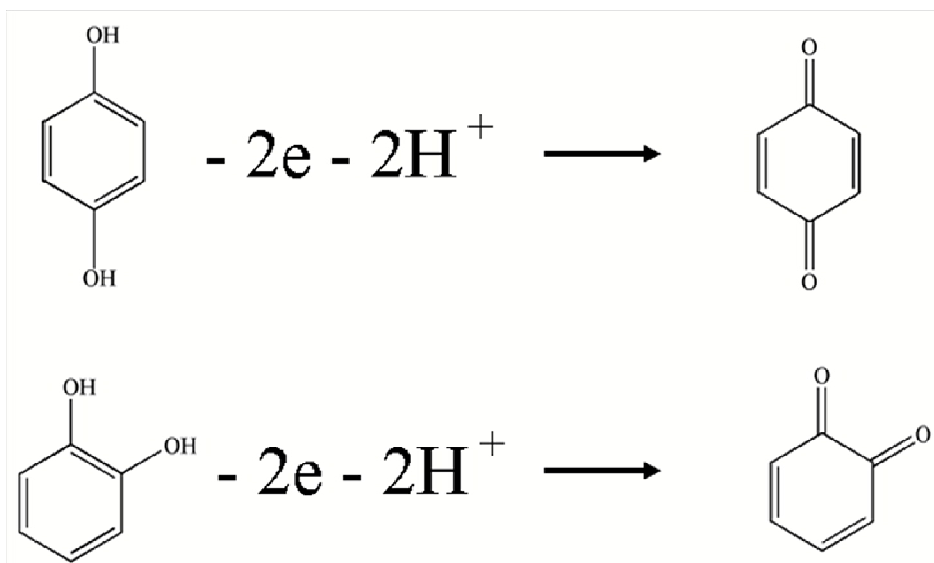
19

20

21

22

1 Scheme 1



2

3

4

5

6

7

8

9

10

11

12

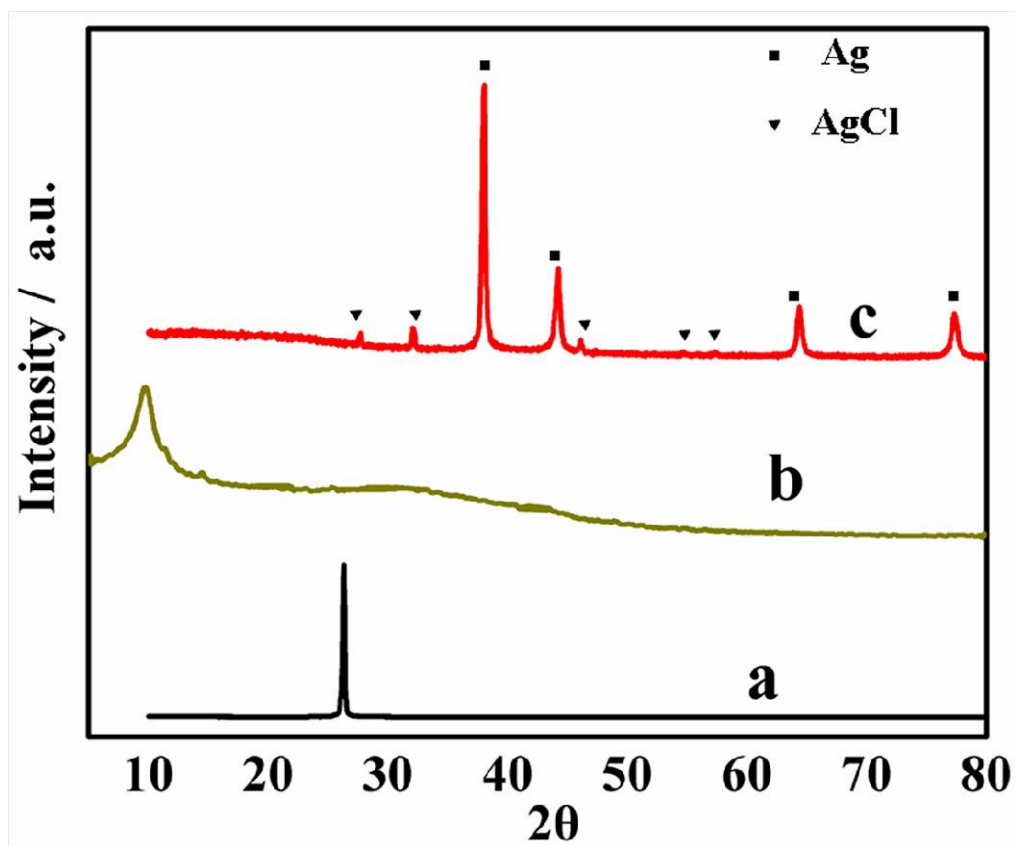
13

14

15

16

1 Fig. 1



2

3

4

5

6

7

8

9

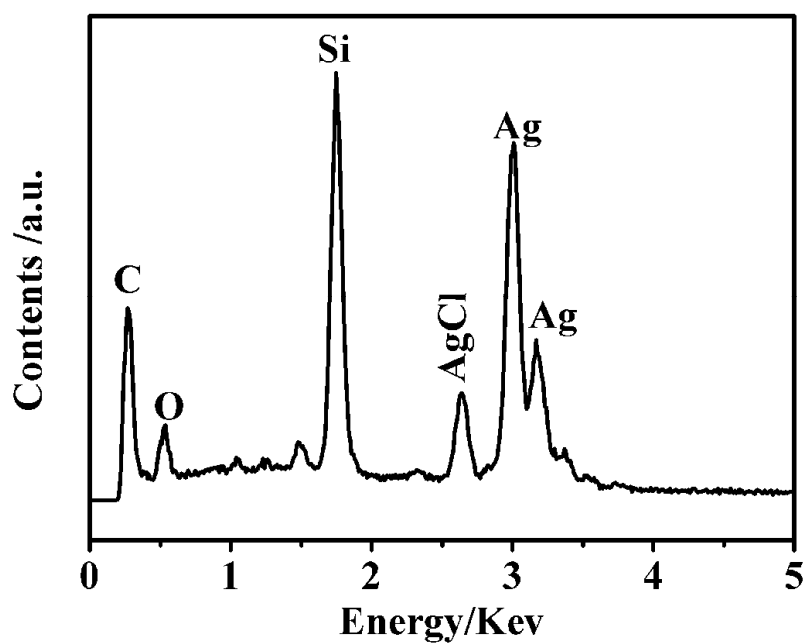
10

11

12

13

1 Fig. 2



2

3

4

5

6

7

8

9

10

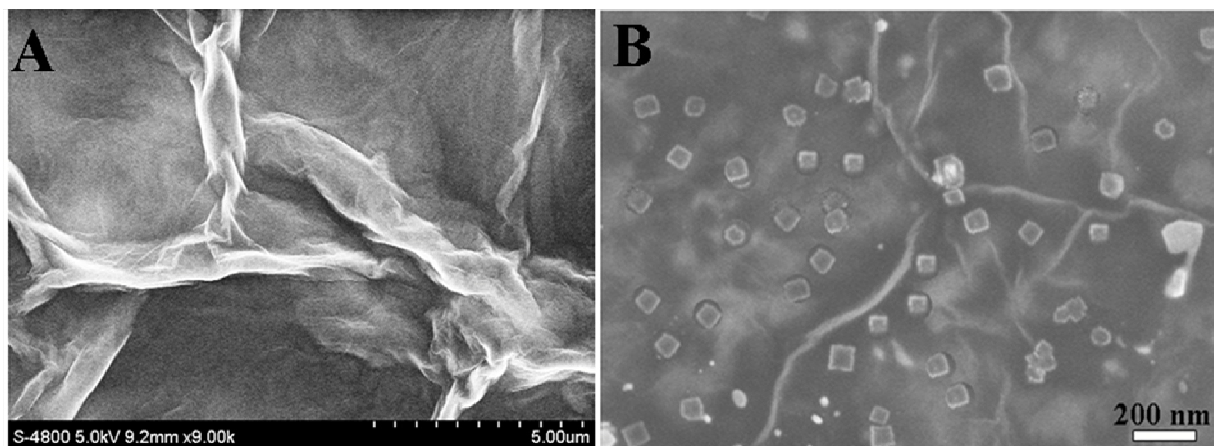
11

12

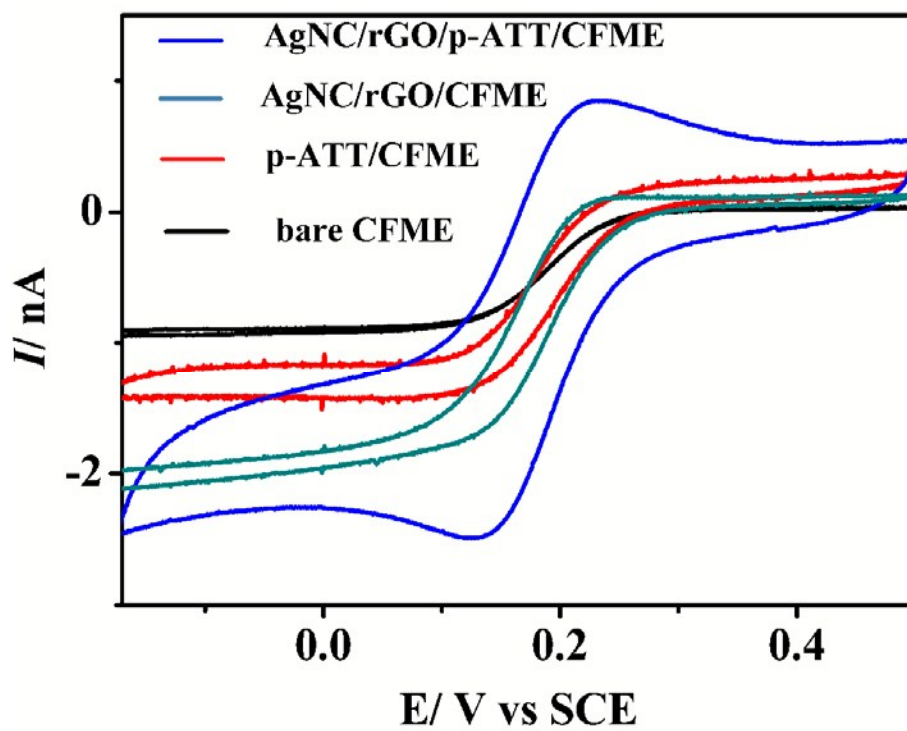
13

14

1 Fig. 3



1 Fig. 4



2

3

4

5

6

7

8

9

10

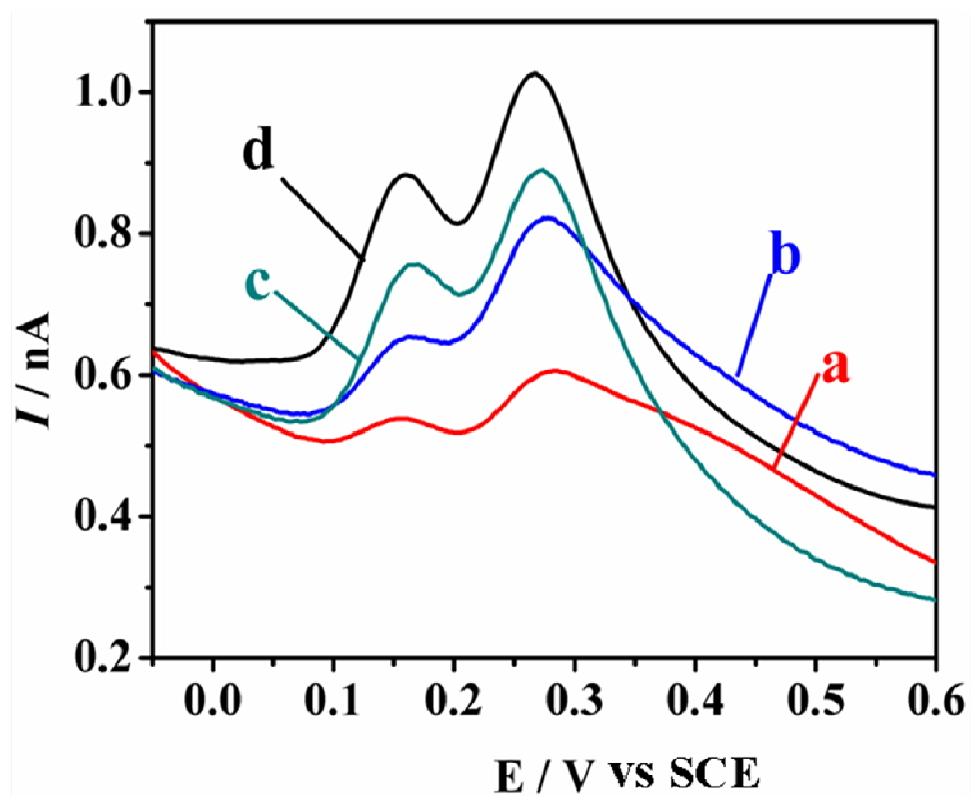
11

12

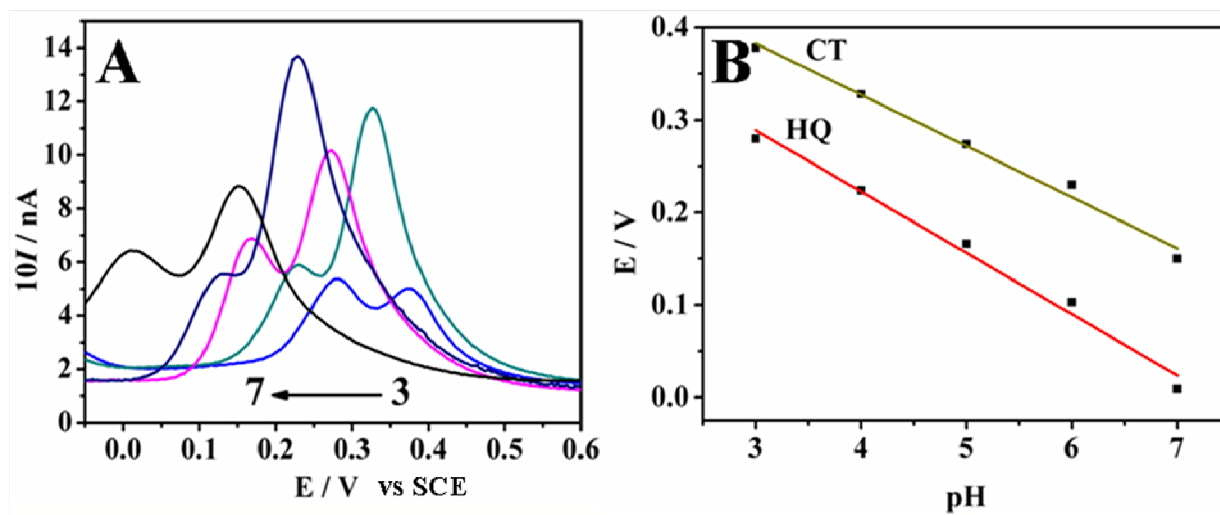
13

14

1 Fig. 5



1 Fig. 6



2

3

4

5

6

7

8

9

10

11

12

13

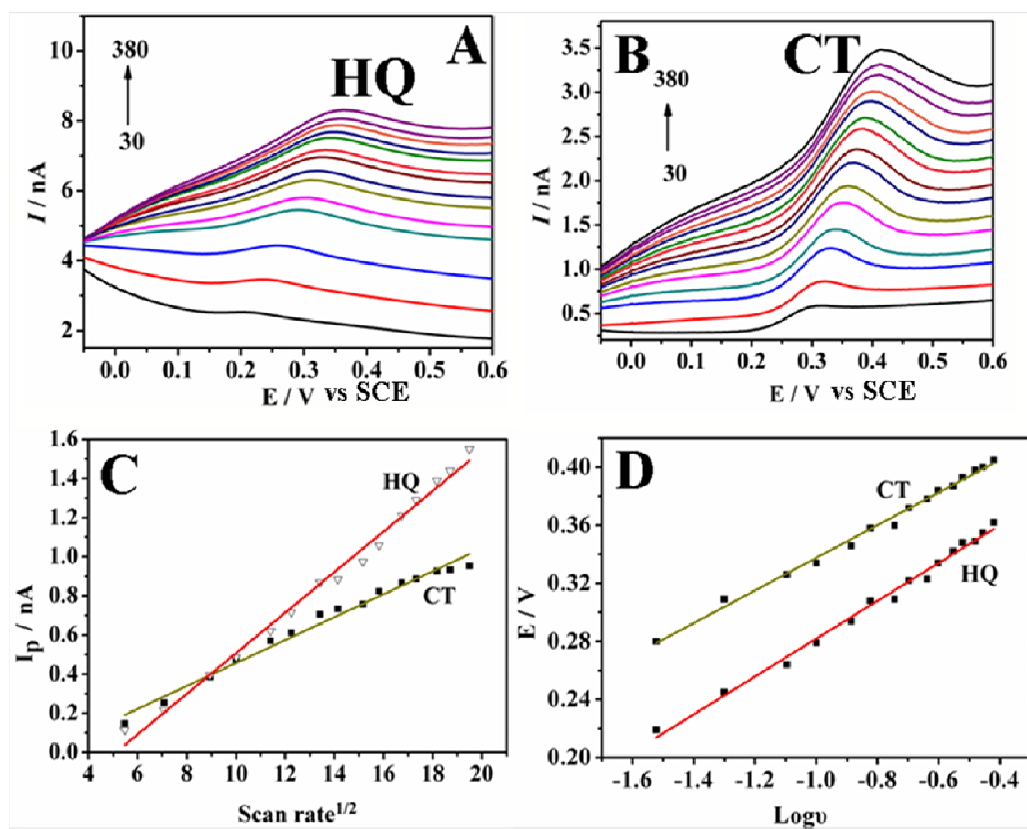
14

15

16

17

1 Fig. 7



2

3

4

5

6

7

8

9

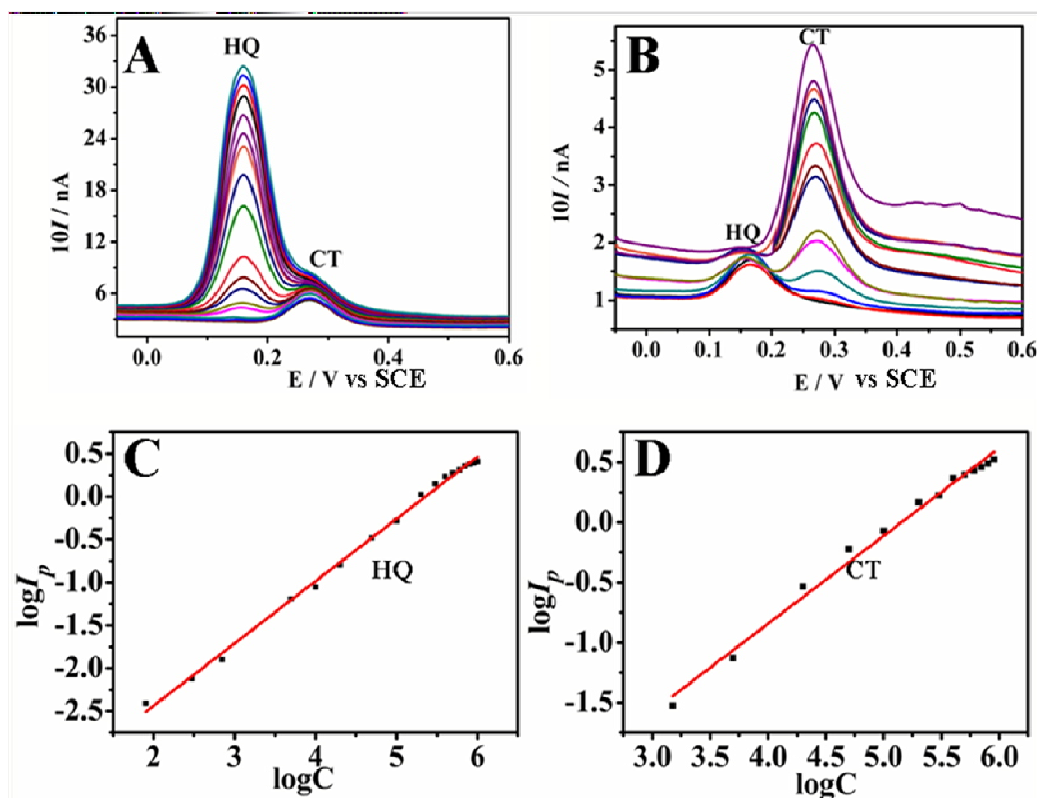
10

11

12

13

1 Fig. 8



2

3

4

5

6

7

8

9

10

11

12

13

1 **Table 1**

2

	HQ	CT
s_b	0.002	0.031
m	0.725	0.731
detection limit($\mu\text{mol L}^{-1}$)	0.0094	0.13

3

4

5

6

7

8

9

10

11

12

13

14

15

16

17

18

19

1 **Table 2**

2

Electrode	Linear range	$(\mu\text{mol L}^{-1})$		LOD	$(\mu\text{mol L}^{-1})$		RSD	Ref.
		HQ	CT		HQ	CT		
IL-rGO ^a /GCE	1-300	8.0-391	0.85	2.6	—	—	—	32
rGO-MWNTs/GCE	2-400	5.55-40	1.0	1.8	0.994	0.992	—	33
carbon electrode	2-50	5-50	2	5	0.996	0.997	—	35
PANI ^b /MnO ₂ /GCE	0.2-100	0.2-100	0.13	0.16	0.997	0.997	—	52
PEDOT ^c /GO/GCE	25-200	2-400	1.6	1.6	0.998	0.999	—	53
PARS ^d /CS/BCN-GO/GCE	1-100	1-100	0.19	0.11	0.997	0.997	—	54
PDA ^e -rGO/GCE	1-250	1-230	0.62	0.74	0.996	0.999	—	55
pyridinic-rGO ^f /GCE	5-30; 30-200	5-200	0.38	1	0.996	0.998	—	56
CdS/rGO/GCE	0.2-2300	0.5-1350	0.054	0.09	0.995	0.997	—	57
AgNC/rGO/p-ATT/CFME	0.08-1000	1.5-900	0.0094	0.13	0.997	0.991	—	This work

3 ^a IL-rGO: ionic liquids -functionalized graphene.4 ^b PANI: polyaniline.5 ^c PEDOT: poly(3,4-ethylenedioxy-thiophene).6 ^d PARS: polymeric alizarin red S.7 ^e PCV: poly(crystal violet).

8

9

10

1 **Table 3**

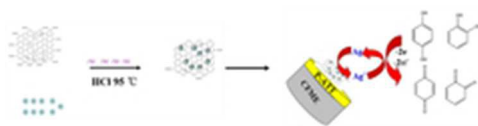
2

Sample	Added ($\mu\text{mol L}^{-1}$)		Found ^a ($\mu\text{mol L}^{-1}$)		Recovery (%)	
	HQ	CT	HQ	CT	HQ	CT
Tap water	50.0	70.0	48.0	70.8	96.0	101.1
Tap water	100.0	120.0	98.4	122.2	98.4	101.8
Lake water	60.0	70.0	61.4	72.2	102.3	103.1
Lake water	100.0	130.0	102.5	133.1	102.5	102.4

3

4

5



20x5mm (300 x 300 DPI)